Article

Characteristic and Catalytic Performance of Co and Co-Mo Metal Impregnated in Sarulla Natural Zeolite Catalyst for Hydrocracking of MEFA Rubber Seed Oil into Biogasoline Fraction

Junifa Layla Sihombing [1,2], Saharman Gea [3],[*] , Basuki Wirjosentono [3], Harry Agusnar [3], Ahmad Nasir Pulungan [2], Herlinawati Herlinawati [2], Muhammad Yusuf [2] and Yasir Arafat Hutapea [3]

[1] Postgraduate School, Department of Chemistry, Faculty of Mathematics and Natural Sciences, Universitas Sumatera Utara, Jl. Bioteknologi No. 1, Medan 20155, Indonesia; junifalaylasihombing@unimed.ac.id

[2] Department of Chemistry, Faculty of Mathematics and Natural Sciences, Universitas Negeri Medan, Jl. Willem Iskandar Pasar V Medan Estate, Medan 20221, Indonesia; nasirpl@unimed.ac.id (A.N.P.); herlinazalfa77@gmail.com (H.H.); yusuf.6423@gmail.com (M.Y.)

[3] Department of Chemistry, Faculty of Mathematics and Natural Sciences, Universitas Sumatera Utara, Jl. Bioteknologi No. 1, Medan 20155, Indonesia; basuki@usu.ac.id (B.W.); harryagusnar@yahoo.com (H.A.); arafatyasir195@gmail.com (Y.A.H.)

[*] Correspondence: s.gea@usu.ac.id

check for updates

Abstract: This research was aimed to investigate the effect of Co and Co-Mo metal loaded on Sarulla Natural Zeolite which has been activated and calcined (SNZ-Cal) as supports for better understanding of characterization and catalytic activity on hydrocracking of MEFA rubber seed oil. The Co and Co-Mo metal was added through a wet impregnation method using $Co(NO_3)_2 \cdot 6H_2O$ and $(NH_4) \cdot 6Mo_7O_{24} \cdot 4H_2O$ precursor salts. The catalyst was oxidized at 500 °C for 2 h within oxygen gas flow, followed by a reduction process with H_2 gas flow with similar condition to obtain the catalysts. Based on the result, it was found that the resulted catalysts displayed an increase in crystal grain size compared to the metal-free catalyst. Particularly, catalyst that was impregnated with Co metal has a larger surface area and pore diameter and smaller pore volume than Co-Mo metal impregnated to the catalyst. In fact, it was revealed that this catalyst possessed the highest catalytic activity and selectivity. Furthermore, the resulting gas products reached 64 wt.% and the distribution of biogasoline fraction of hydrocarbons (C6-C12) amounted to 83.19 wt.%.

Keywords: sarulla natural zeolite; MEFA; hydrocracking; catalyst activity and selectivity; biogasoline

1. Introduction

Biofuel production from vegetable oil has enormous potential as an alternative energy source to replace fossil fuels. In addition, biofuels are environmentally friendly since they are free from nitrogen and sulfur compounds. Biofuel can be obtained from biomass and agricultural or plantation products such as palm, vegetable, soybean, and rubber seed oil [1]. Rubber seed oils are non-edible oils obtained from rubber seeds; whose availability is very abundant in Indonesia but not yet optimally utilized. The rubber seed oils contain the main linoleic acid 39 of 67% and oleic acid of 23.52% [2].

Several methods can be used to convert vegetable oils into biofuels, such as pyrolysis, gasification, and trans-esterification, catalytic cracking reaction and hydrocracking reaction [3–7]. Catalytic cracking [8] and hydrocracking reaction [7] are one of the technologies that are widely used to

produce biofuels sourced from vegetable oils. In thermal cracking reactions, high molecular weight hydrocarbons can be converted into hydrocarbon compounds with a lighter molecular weight through thermolysis at high temperatures, followed by coke formation, a large amount of gas and naphtha of low quality as a result of the over-cracking process so that this process is not desirable.

On the other hand, the use of catalysts in the cracking process can reduce the decomposition temperature, because it reduces the activation energy of the cracking [9], therefore, it will make the whole process more efficient because it reduces pollution with lower energy consumption and minimizes unnecessary byproducts, like heteroatom substances [10]. In the hydrocracking process, high molecular weight hydrocarbons are converted into hydrocarbon compounds with a lighter molecular weight with simultaneous or sequential hydrogenation and carbon bond breaking [9]. In recent years, various types of heterogeneous catalysts have been used as catalysts for these processes, such as HZSM-5 [11,12], MCM-41 [13], CaO [8], and multi porous composite MC-ZSM-5/MCM-41 [1]. The products produced are generally having low viscosity and high cetane number (>50). Besides that, they also have physical and chemical properties that are compiled to those specified for petroleum-based fuels.

Zeolite has been considered as one of the most important catalysts in the petrochemical industry because of its excellent chemical properties [14,15] to act as a catalyst, such as acidity, thermal stability, and having pores of sufficient size to allow reactants to access the surface. On the other hand, Indonesia is known as a country to dominate natural zeolite reserves, spread on the islands of Sumatra, Java, and Sulawesi with 447,490,160 tons in amount [16]. The distribution of natural zeolite on Sumatra Island is mainly found in Lampung and North Sumatra regions. In particular, natural zeolite deposits range from 16,200,000 tons was discovered in North Sumatra. In fact, this natural reserve is very potential to be used as a catalyst material. A characterization of Sarulla natural zeolite crystal and its morphological structure has been performed by Sihombing et al. (2018) [17]. Moreover, the data reported that natural zeolite which was treated with activation and calcination (SNZ-Cal) process resulted good crystallinity, thermal stability, and surface area. In addition, SNZ-Cal catalyst activity test results for the rubber seed oil hydrocracking process showed a fairly good catalytic activity with the conversion value of liquid products reaching 80.60%. However, the product selectivity for the bio gasoline fraction was obtained for less than 50% [18].

Many researchers have tried to modify the zeolite to obtain the optimum amount and strength of the acid site in the zeolite and also the appropriate pore structure that has high activity and selectivity, namely by impregnating the transition metals into the pore. Cobalt (Co) and molybdenum (Mo) metals have been combined with alumina as a catalyst for the hydrocracking and hydro treating processes of heavy oils. This catalyst has shown a lower level of coke and higher conversion [19–21]. As it is known, the formation of coke in the hydrocracking process can deactivate the active catalyst site, so that the catalyst activity decreases.

Therefore, this research aims to reveal the activity and selectivity of Co and Co-Mo catalysts impregnated in zeolite carriers for hydrocracking of MEFA rubber seed oils to biofuel. In addition, the effect of the combination of metal catalysts on the product and the selectivity of liquid products produced on the Bio gasoline and biodiesel fractions are also studied.

2. Results and Discussion

The administration of a metal catalyst in the SNZ-Cal carrier was aimed to improve the character of zeolite catalyst that has an effect on increasing the activity and selectivity of the catalyst in the rubber seed oil hydrocracking process. In a metal catalyst/carrier system or often referred to as a bi-functional catalyst, acid and metal sites are commonly consisted. The acid site is contained in the SNZ-Cal carrier material (which consists of the Bronsted and Lewis acid sites). In contrast, the metal site is in the transition metal used, Co and the Co-Mo combination. Transition metals are chosen as catalysts because they provide empty d orbitals, resulting in an effective ability to receive electron pairs from the reactants to undergo a reaction [22].

2.1. Catalysts Characteristics

In order to observe the effect of Co metal and Co-Mo metal combination loading on SNZ-Cal carrier, a comparison of the characteristic peaks of XRD diffractogram of each catalyst with the main peaks of SNZ-Cal carrier at an angle of 2θ (degrees) was carried out. The comparison of each catalyst diffractogram is presented in Figure 1. SNZ-Cal diffractogram reveals that the carriers contain clinoptilolite, mordenite, and quartz crystals with amorphous and crystalline phases. In addition, same result was reported by Gultom et al. (2016) [23]. The main diffractogram peaks that confirm the presence of zeolite are at $2\theta = 20.10°$, $22.05°$, $28.46°$, $29.70°$ (clinoptilolite phase), and $2\theta = 24.49°$, $25.68°$, $27.88°$, $35.70°$ (modernite phase).
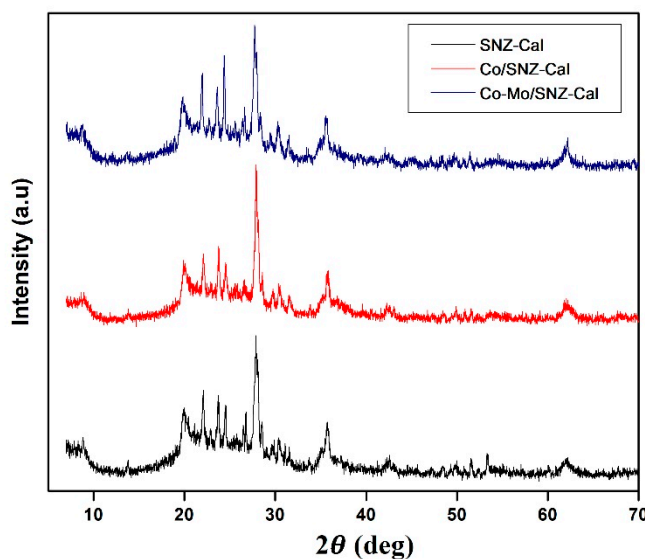
Figure 1. XRD analysis result of SNZ-Cal, Co/SNZ-Cal, and Co-Mo/SNZ-Cal catalysts.

In the SNZ-Cal carrier, Co and Co-Mo metal loading did not indicate a significant decrease in the intensity of the peak. Besides that, the intensity ratio of the main peaks of each catalyst is formed at an angle of 2θ (degrees) that are almost the same. Although it displays different intensities, same diffractogram pattern was obtained. Overall, it can be concluded that the loading of Co and Co-Mo metals in SNZ-Cal holders does not damage the zeolite crystal structure. The loading of Co and Co-Mo metals is evenly distributed in the SNZ-Cal pore, added with no sintering that can cover the active site of the catalyst. Sriningsih et al. (2014) reported that double metal carriers in active natural zeolites did not damage the zeolite crystal structure, although the peak intensity was observed to be lower than the single metal catalysts [9].

Based on the results, the diffraction peaks of Co metal oxides were recorded at $2\theta = 42.40°$, $36.50°$, dan $61.52°$. However, Sadek et al. (2019) reported that the oxide phase of Co metal was observed at $2\theta = 36.80°$, $59.30°$, dan $65.20°$ [24]. On the other hand, the diffraction peaks for Mo metal were reported at $2\theta = 57.76°$ and $72.87°$ [25].

Specific diffraction peaks to Co and Mo metals were not observed in the diffractogram of the Co/SNZ-Cal and Co-Mo/SNZ-Cal catalysts. This is caused by only a small amount of Co and Co-Mo metals that were embedded in SNZ-Cal bearers. In particular, Table 1 describes the presence of Co metal on the Co/SNZ-Cal catalyst that was only 0.76%. This value is smaller than it should be theoretically calculated at 1%. While on the Co-Mo/SNZ-Cal catalyst, Co metal was detected at 0.58%, which is a value in accordance with theoretical calculations, but the presence of Mo metal is still very small. Another possibility to this issue is due to low phase of resistance, resulting an unreadable peak of diffraction. The same case has been reported by Perez et al. (2011), who discovered that the Fe metal

loaded into the carbon-supported catalysts at an amount of 20 wt.% was not observed by XRD analysis, as a result the metal formed a stable structure but not crystalline [26].

Table 1. Metal load of the SNZ-Cal supported catalysts.

Catalysts	% Metal (wt.) *	
	Co	**Mo**
SNZ-Cal	-	-
Co/SNZ-Cal	0.76	-
Co-Mo/SNZ-Cal	0.58	0.002

* SEM-EDX analysis.

Furthermore, in order to observe the effect of metal loading on the crystallinity of the catalyst in more detail, it is determined based on the changes in the value of full width at half maximum (FWHM) peak X-ray diffraction intensity for a particular orientation field. The average value of crystal grain size calculated by the Debye–Scherrer equation is shown in Equation (1) [27].

$$D = 0.9 \; \lambda/B \; \mathrm{Cos}\theta \tag{1}$$

where:

D = Average size crystal grain
λ = X-ray wavelength (0.15406 nm)
θ = Braag degree angle
B = FWHM value in radii
The result of crystal size measurements for each catalyst is described in Table 2.

Table 2. Crystal grain size of SNZ-Cal, Co/SNZ-Cal, and Co-Mo/SNZ-Cal catalysts.

SNZ-Cal		Co/SNZ-Cal		Co-Mo/SNZ-Cal	
2θ (Degree)	D (nm)	2θ (Degree)	D (nm)	2θ (Degree)	D (nm)
27.88	16.103	27.92	19.038	27.76	17.482
23.70	22.944	23.76	29.288	23.57	23.275
22.04	21.149	22.08	24.661	21.90	24.203
20.10	9.028	20.05	11.160	19.90	9.909

Based on Table 2, it can be seen that in the Co/SNZ-Cal and Co-Mo/SNZ-Cal catalysts, an increase in crystal grain size was found compared to SNZ-Cal. This relates to decreasing porosity (pore size) and catalyst surface area as a result of administration process of Co metal and the combination of Co-Mo metals in the catalyst pore. This data correlates with the results of measurements of surface area, total volume, and pore diameter of each, which is presented in Table 3.

Table 3. Specific surface area, pore volume and average pore diameter of SNZ-Cal, Co/SNZ-Cal, and Co-Mo/SNZ-Cal catalysts.

Catalysts	Surface Area (m^2/g) *	Pore Volume (cc/g) *	Pore Diameter (nm) *
SNZ-Cal	107	0.23	4.27
Co/SNZ-Cal	96	0.19	3.96
Co-Mo/SNZ-Cal	86	0.22	5.07

* BET analysis.

Surface area, pore volume, and average pore diameter are important characteristics of the catalyst that greatly influence the activity and selectivity of the catalyst. The data in Table 3 illustrates that the development of a single Co metal and a combination of Co-Mo metals results in a reduction in the specific surface area of the catalyst. This is possible since the more impregnated metal into the pores of the carrier, the pores of the carrier with smaller fingers will be blocked, so that the surface area of the catalyst decreases but the mean of the pore radius increases. The larger pore network indicates that the metal/catalyst system of Co/SNZ-Cal and Co-Mo/SNZ-Cal has a fairly large inter-pore space. Catalyst with a large pore size is very important for the catalytic reaction process, which allows reactant particles to interact with the catalyst to the pore inside the catalyst. This allows reactions to occur on the surface of a larger catalyst.

The effect of the administration of a metal catalyst on the adsorption-desorption isotherms of each catalyst is presented in Figure 2. The comparison of the adsorption isotherms of the SNZ-Cal, Co/SNZ-Cal and Co-Mo/SNZ-Cal catalysts in Figure 2 describes that each catalyst has a hysteresis loop shape with comparable adsorption and desorption capabilities. Nevertheless, it can be seen that the Co/SNZ-Cal and Co-Mo/SNZ-Cal catalysts indicate lower nitrogen gas adsorption volumes compared to SNZ-Cal catalysts. The shape of the isotherm desorption graph in Figure 2 has been reported as a type C graph based on Brunauer-Emmett-Teller (BET) calcification [17].
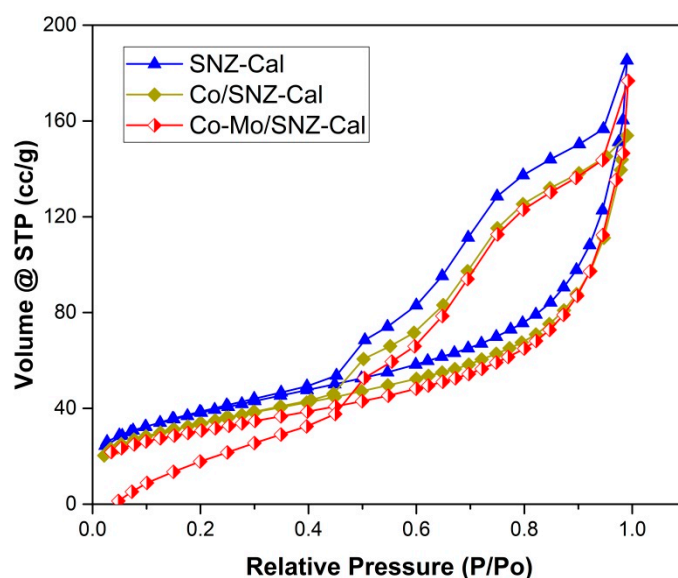

Figure 2. The comparison of isothermal adsorption-desorption nitrogen gas from SNZ-Cal, Co/SNZ-Cal, and Co-Mo/SNZ-Cal catalysts.

The comparison of pore size distribution of each catalyst is shown in Figure 3. The dV(r) (differential volume radius) value represents the pore distribution of the catalyst. The greater the value of dV(r) at each pore diameter, the more the pore is distributed to the catalyst. Figure 3b shows that Co/SNZ-Cal and Co-Mo/SNZ-Cal catalysts have dV(r) value decreased compared to SNZ-Cal as a result of impregnation of Co metal and combination of Co-Mo metals in the catalyst pore. Furthermore, Figure 3 indicates that the pore size distribution of each catalyst is dominated in the same region, between 20 Å–100 Å.

The results of SEM imaging of each catalyst are shown in Figure 4. The morphology and surface topology of each catalyst were analyzed with SEM at a magnification of 2000 times. In Figure 4b, it is observed that Co metal in Co/SNZ-Cal catalyst was distributed more homogeneously on the surface and pore of the catalyst. The metal can be dispersed evenly throughout the zeolite pore system, so that an active metal surface is produced [28]. While in Figure 4c, the Co-Mo/SNZ-Cal catalyst shows that the combination of Co and Mo metal forms a larger aggregate on the zeolite (SNZ-Cal) carrier surface. This is likely to occur because the Mo metal which is first placed, is located more on the outermost surface of the zeolite carrier. This is in line with the report of [29] which stated that Mo metal is more dispersed
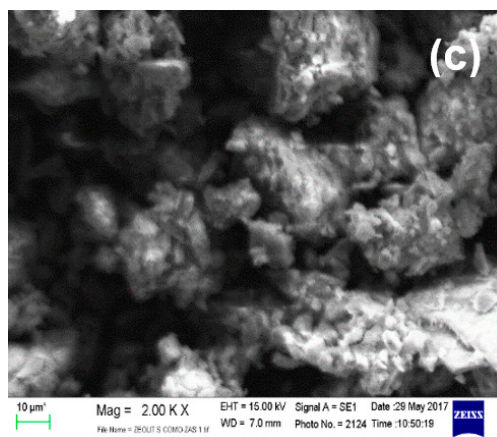
on the carrier surface. It is because the loaded Co metal is difficult to enter the zeolite carrier pore. Metals Co and Mo are likely to intersect into larger aggregates and are likely to form external pores.
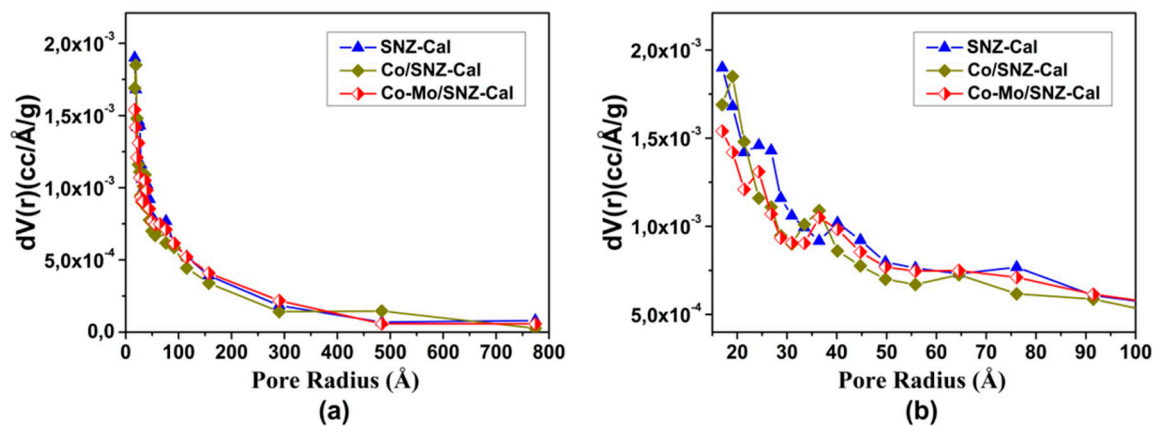
Figure 3. Pore size distribution using BJH method of SNZ-Cal, Co/SNZ-Cal, and Co-Mo/SNZ-Cal catalysts with the range of (**a**) 0–800 Å and (**b**) 20–100 Å.
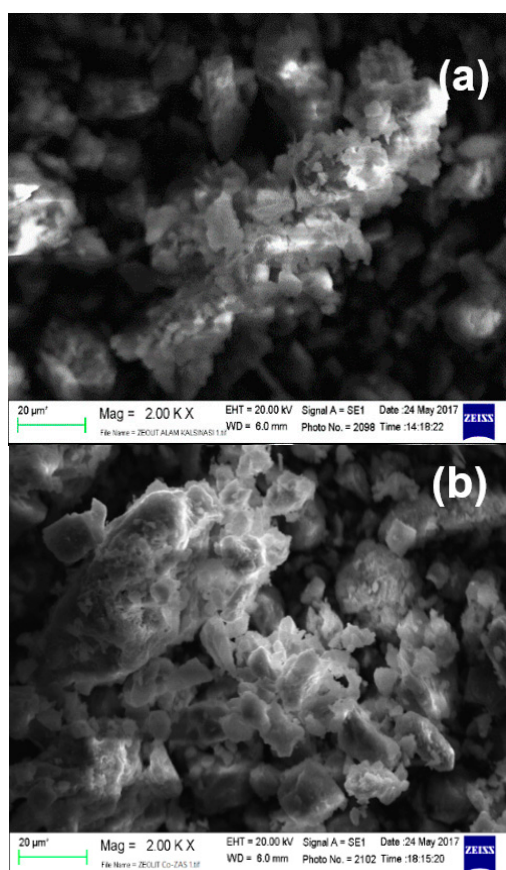

Figure 4. *Cont.*

Figure 4. SEM morphological imaging results with 2000 times magnification of (**a**) SNZ-Cal, (**b**) Co/SNZ, and (**c**) Co-Mo/SNZ catalysts.

## 2.2. Catalytic Performance of Catalysts

The activity test of each SNZ-Cal, Co/SNZ-Cal, and Co-Mo/SNZ-Cal catalyst was carried out in the MEFA hydrocracking process for rubber seed oil. In the heterogeneous reaction process, the reactants in the reaction system are not in the same phase, therefore in this research, the heterogeneous system uses the gas phase as reactants. The mechanism of MEFA hydrocracking process for rubber seed oil with SNZ-Cal, Co/SNZ-Cal, and Co-Mo/SNZ-Cal catalysts are illustrated in Figure 5. In a heterogeneous reaction system, the reaction occurred involves the reaction of adsorption processes and desorption of reaction products from the catalyst surface. In the initial stage of the reaction, the reactant molecules must be diffused to the surface of the catalyst, followed by the adsorption process of the reactant molecules on the catalyst surface. The next stage is the hydrocracking reaction of reactant molecules to produce a product followed by the process of desorption of product molecules from the surface of the catalyst. In the final stage, the process of transferring the hydrocracking product to the fluid phase is conducted.
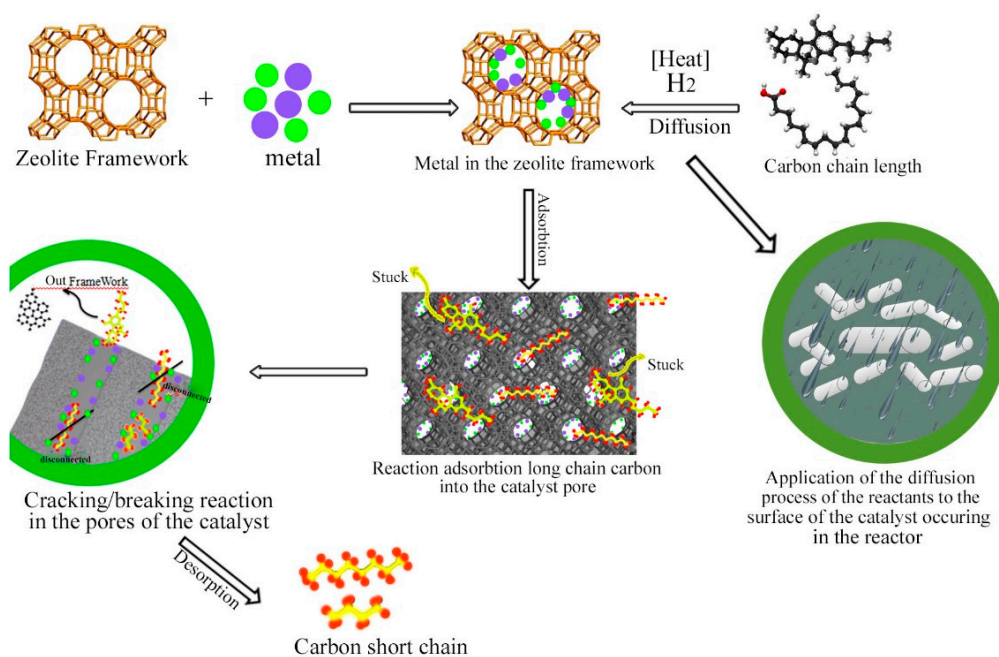
Figure 5. The process scheme of MEFA rubber seed oil catalytic cracking MEFA using zeolite with metal-catalyst loading system.

In previous studies, an activity test of the SNZ-Cal catalyst was obtained [18]. The optimum conditions were obtained with the acquisition of 80.60 wt.% liquid product, 3.20 wt.% of coke, 15 wt.% of gas, and 1.2 wt.% of residue at 500 °C reaction temperature and feed catalyst ratio of 0.5 (*w/w*). To see the effect of the metal catalyst used on the catalytic performance, a comparison of the results of the catalyst activity of Co/SNZ-Cal and Co-Mo/SNZ-Cal on SNZ-Cal on the same conditions and process is presented in Figure 6.

Figure 6 describes the comparison of the catalytic activity of catalysts of Co/SNZ-Cal and Co-Mo/SNZ-Cal against SNZ-Cal. The presence of a metal catalyst applied to SNZ-Cal increases the catalytic activity of the catalyst. This can be seen from the increase in gas produced. The gas produced by the catalyst of Co/SNZ-Cal is greater in amount compared to Co-Mo/SNZ-Cal and SNZ-Cal. In particular, Co/SNZ-Cal catalyst gives a greater gas product than Co-Mo/SNZ-Cal catalyst, which is 64%. This indicates that Co/SNZ-Cal catalyst has higher cracking catalytic activity than SNZ-Cal catalyst. This is possible because the inclusion of Co metal in the carrier pore gives more active sites to play a role in the reaction process, so that the probability of a reaction occurring in the active site is greater. The existence of the zeolite Bronsted acid site and the metal active site cause the Co/SNZ-Cal catalyst to have more active catalytic properties. The empty d orbitals owned by the condensed metal function as Lewis acid sites that can accept electron pairs from the reactants, therefore breaking the C-C bond occurs through the carbocation mechanism. In addition, in terms of the specific surface area of the catalyst, the Co/SNZ-Cal catalyst has a larger surface area than Co-Mo/SNZ-Cal, but a smaller pore diameter and pore volume. With such characteristics, the Co/SNZ-Cal catalyst produces a better reaction on the catalyst surface and is able to maintain the short chain hydrocarbons formed. This phenomenon may be caused by siltation of a number of pores by metal particles resulting in the position of metal particles in the pore, allowing effective cracking of the hydrocarbon fraction, thereby increasing the gas products. Meanwhile, in Co-Mo/SNZ-Cal catalyst with a pore diameter greater than Co/SNZ-Cal catalyst, mass transfer might occur in the hydrocracking process, reducing catalytic activity. This can be seen from the lower gas product produced by 25 wt.% with liquid products and residues by 52 wt.% and 22.20 wt.% respectively.
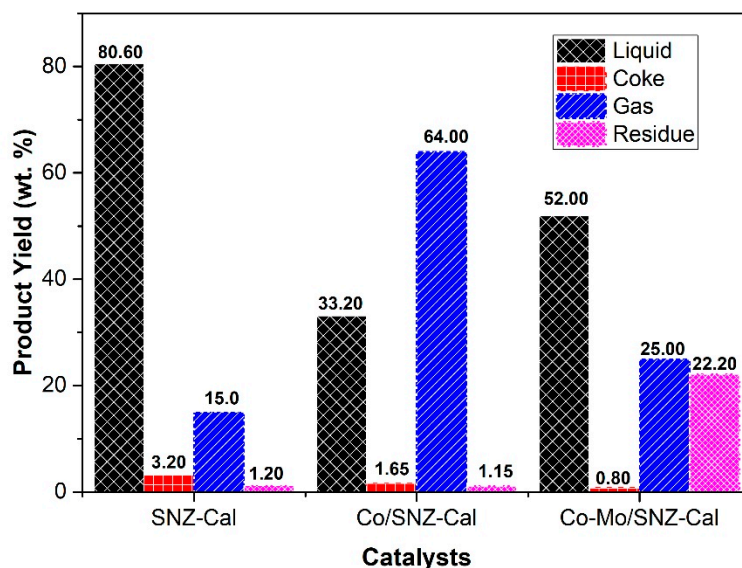

Figure 6. The yield of products from MEFA rubber seed oil hydrocracking over SNZ-Cal, Co/SNZ-Cal, and Co-Mo/SNZ-Cal catalysts.

Based on the GC chromatogram in Figure 7, it can be observed that in the initial state, the hydrocarbon compounds from MEFA were at retention times over 15 min. After experiencing cracking reaction, hydrocarbon compounds were observed to shift at a retention time of less than 15 min. The peak intensity of the highest hydrocracking compound was produced by the Co/SNZ-Cal catalyst.

Furthermore, Figure 7 shows that the Co/SNZ-Cal and Co-Mo/SNZ-Cal catalysts are more selective on the C_6-C_{12} carbon fraction compared to SNZ-Cal. The pore size of the smaller Co/SNZ-Cal and Co-Mo/SNZ-Cal catalysts will limit the formation of long and brittle carbon chains. Comparison of the distribution of hydrocarbon compounds in the bio gasoline fraction (C_6-C_{12}), biodiesel fraction (C_{12}-C_{20}) and >C_{20} fraction of each catalyst is displayed in Figure 8.
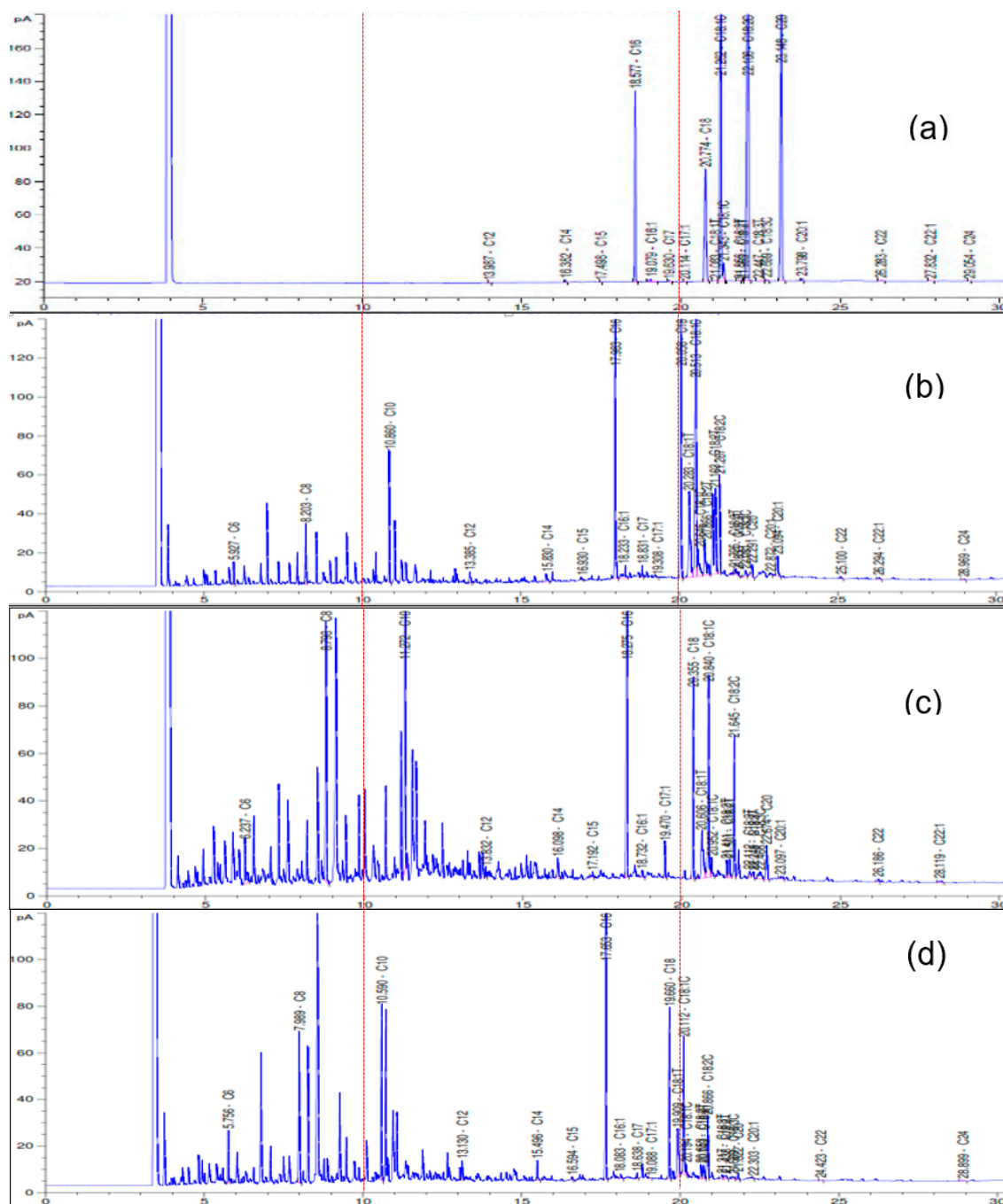

Figure 7. The comparison of GC chromatogram of (**a**) MEFA rubber seed oil, and liquid product result of MEFA rubber seed oil hydrocracking over catalyst, (**b**) SNZ-Cal, (**c**) Co/SNZ-Cal, and (**d**) Co-Mo/SNZ-Cal catalysts.

The distribution of the hydrocarbon compound fraction from the liquid product in Figure 8 shows that the addition of Co metal and the Co-Mo metal combination contribute to the increase in selectivity

of liquid product to the bio gasoline fraction (C_6-C_{12}). The Co-SNZ-Cal and Co-Mo/SNZ-Cal catalyst systems produce hydrocarbon compounds of bio gasoline fraction (C_6-C_{12}) with a greater amount than diesel fraction (C_{12}-C_{20}) and >C_{20} fraction. The highest bio gasoline fraction product was produced by Co/SNZ-Cal catalyst with a value of 83.19 wt.% followed by Co-Mo/SNZ-Cal, SNZ-Cal catalyst at 78.96 wt.% and 37.31 wt.% respectively. Trisunaryanti (2013) reported that by using zeolite that was carried by metal, it would produce a liquid product with fraction of C_7-C_{12} [22]. The composition of the hydrocarbon compound from the bio gasoline fraction produced by each catalyst is shown in Figure 9. Based on this figure, it can be seen that the Co metal and the Co-Mo metal combination applied to the SNZ-Cal catalyst solids influence the distribution of hydrocarbon compounds composition. In addition, the distribution of hydrocarbon compounds in bio gasoline fraction is strongly influenced by the pore size of the catalyst [30–32].
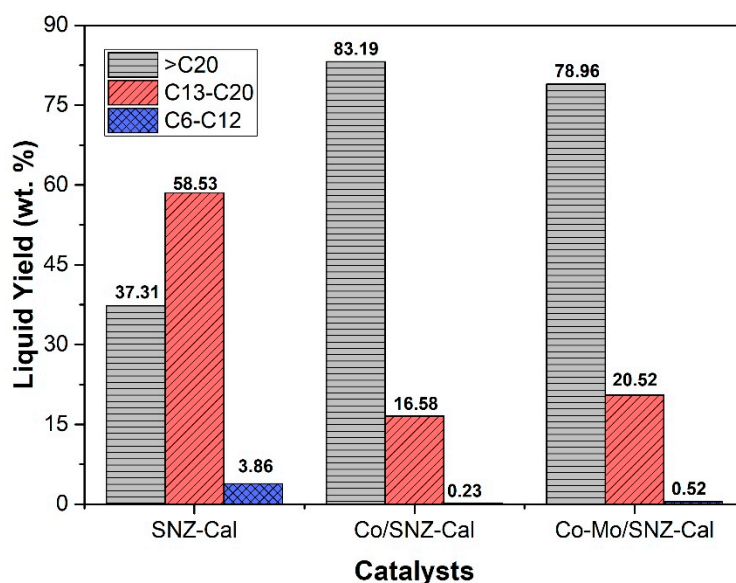
Figure 8. Liquid products composition obtained from the hydrocracking of MEFA rubber seed oil over SNZ-Cal, Co/SNZ-Cal, and Co-Mo/SNZ-Cal catalysts.
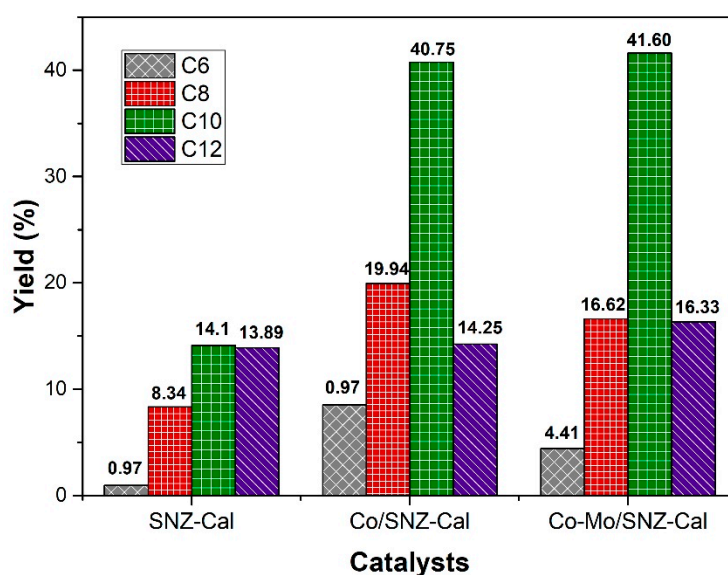
Figure 9. The percentage of carbon fraction over biogasoline fraction resulted by SNZ-Cal, Co/SNZ-Cal, and Co-Mo/SNZ-Cal catalyst.

3. Materials and Method

3.1. Materials

MEFA rubber seed oil, natural zeolite was obtained from Sarulla (Jakarta, Indonesia), Indonesia. Precursor metal of $Co(NO_3)_2 \cdot 6H_2O$ and $(NH_4)_6Mo_7O_{24} \cdot 4H_2O$ were purchased from Merck (Kenilworth, NJ, USA). Lastly, distilled water was purchased from Bratachem (Jakarta, Indonesia) while hydrogen, oxygen, and nitrogen gas were purchased from PT. Aneka Gas, Medan, Indonesia.

3.2. Preparation of Sarulla Natural Zeolite-Calcination (SNZ-Cal)

The SNZ-Cal material was prepared following a procedure that had been performed by Sihombing et al. (2018) [18]. Sarulla natural zeolite (SNZ) was crushed to pass through 100 mesh, then washed with distilled water and dried in an oven at a temperature of 120 °C. SNZ was then activated with 3N HCl acid reflux method at 90 °C for 1 h. Then, it was washed with distilled water to reach a neutral pH of 7 and dried in the oven. Lastly, SNZ was calcined at a temperature of 500 °C, with Nitrogen gas flow for 2 h to obtain SNZ-Cal.

3.3. Preparation of Co/SNZ Catalyst

A total of 1% (*w/w*) $Co(NO_3)_2 \cdot 6H_2O$ was added into an amount of 100 g of SNZ-Cal using wet impregnation method. Then, the mixture was refluxed for 5 h at 80 °C. The mixture was oxidized with oxygen gas (±20 mL/s) flowing for 2 h at a temperature of 500 °C. Then, a reduction process was carried out by flowing hydrogen gas (±20 mL/s) for 2 h at 500 °C to produce Co/SNZ-Cal catalyst.

3.4. Preparation of Co-Mo/SNZ Catalyst

A total of 0.5% (*w/w*) of $(NH_4)_6Mo_7O_{24} \cdot 4H_2O$ was added into 100 g of SNZ-Cal using the wet impregnation method. After that, the mixture was refluxed for 5 h at 80 °C to produce Mo/SNZ-Cal. Then, as much as 0.5% (*w/w*) of $Co(NO_3)_2 \cdot 6H_2O$ was added to Mo/SNZ-Cal. The mixture was refluxed for 5 h at 80 °C, followed by oxidation process with oxygen gas (±20 mL/s) flow for 2 h at a temperature of 500 °C. Lastly, it was reduced using hydrogen gas (±20 mL/s) flow for 2 h at 500 °C to obtain a Co-Mo/SNZ-Cal catalyst.

3.5. Characterization of Catalysts

Several significant properties of SNZ-Cal, Co/SNZ-Cal, and Co-Mo/SNZ-Cal catalysts were characterized by Shimadzu type 8201-FC FTIR spectrometers (Kyoto, Japan). The crystallinity was observed by XRF and XRD analysis methods using X-ray diffractometer, Shimadzu 6100 using Cu Kα radiation at 40 Kv and 30 mA with a scanning rate of 2° min^{-1} in the range of 2θ of 7°–70°. Furthermore, catalyst surface morphology was observed with SEM and SEM-EDX analysis method, using Zeis type EPOMH 10 Zss (Carl Zeiss Group, Germany). Lastly, surface area, total pore volume, and pore diameter were measured with BET method using a Quantachrome NOVA 1200e gas sorption analyzer (Boynton Beach, FL, USA).

3.6. Catalytic Activity Test

Catalytic activity test of Co/ZY and Co-Mo/ZY catalyst on MEFA rubber seed oils catalytic *Hydrocracking* process was conducted in a fix-bed reactor system. The reaction temperature was set at 500 °C and feed:catalyst ratio was 1:2 with a reaction time of 2 h. The conversion yield of each product was calculated using the equation used by Sriningsih et al. (2014) [9] and the resulting liquid products were analyzed through GC and GC-MS (GC-FID Agilent Technologies 6890N Network, Santa Clara, CA, USA) methods.

4. Conclusions

The loading of Co metals and the combination of Co-Mo metals in SNZ-Cal affects the properties and performance of catalyst. The XRD analysis data indicated that impregnation of Co and Mo metals resulted in an increase and also a decrease in the intensity of catalyst main peak, nevertheless did not damage the zeolite crystal structure. Co/SNZ-Cal catalysts produce more homogeneous and regular surface morphology and topology. It is caused by an even distribution of Co metals on the surface and pore bearers. In contrast, the Co-Mo/SNZ-Cal catalyst produces the formation of a larger aggregate on the surface of the catalyst. In fact, Co/SNZ-Cal catalyst showed better performance compared to Co-Mo/SNZ-Cal in the MEFA hydrocracking process of rubber seed oil, where the gas produced by Co/SNZ-Cal was higher than Co-Mo/SNZ-Cal. However, the GC product results showed that the Co/SNZ-Cal catalyst produced a higher distribution of the bio gasoline fraction compared to Co-Mo/SNZ-Cal. In conclusion, it is necessary to perform the need for conformity of pore size and specific surface area to the activity and selectivity of the catalyst during the cracking reaction, including the reactant adsorption process, catalytic cracking process, and the desorption of the cracking molecules from the surface of the catalyst.

References

1. Nam, L.T.H.; Vinh, T.Q.; Loan, N.T.T.; Tho, V.D.S.; Yang, X.-Y.; Su, B.-L. Preparation of Bio-Fuels by Catalytic Cracking Reaction of Vegetable Oil Sludge. *Fuel* **2011**, *90*, 1069–1075. [CrossRef]

2. Wibowo, A.A.; Firdausyah, S.; Hajjah, S.; Dwiyanti, D.; Sihombing, J.L.; Pulungan, A.N. Study of Rubber Seed Oils Hydrocracking into Bio Gasoline and Diesel Fraction over the Combination Y-Zeolite and Ni Catalyst. In *The First International Seminar on Trends in Science and Science Education*; Universitas Negeri Medan: Medan, Indonesia, 2014; pp. 132–140.

3. Suarez, P.A.Z.; Moser, B.R.; Sharma, B.K.; Erhan, S.Z. Comparing the Lubricity of Biofuels Obtained from Pyrolysis and Alcoholysis of Soybean Oil and Their Blends with Petroleum Diesel. *Fuel* **2009**, *88*, 1143–1147. [CrossRef]

4. Zabaniotou, A.; Ioannidou, O.; Skoulou, V. Rapeseed Residues Utilization for Energy and 2nd Generation Biofuels. *Fuel* **2008**, *87*, 1492–1502. [CrossRef]

5. Fabbri, D.; Bevoni, V.; Notari, M.; Rivetti, F. Properties of a Potential Biofuel Obtained from Soybean Oil by Transmethylation with Dimethyl Carbonate. *Fuel* **2007**, *86*, 690–697. [CrossRef]

6. Demirbas, A. Biodiesel Production from Vegetable Oils via Catalytic and Non-Catalytic Supercritical Methanol Transesterification Methods. *Prog. Energy Combust. Sci.* **2005**, *31*, 466–487. [CrossRef]

7. Bezergianni, S.; Kalogianni, A.; Vasalos, I.A. Hydrocracking of Vacuum Gas Oil-Vegetable Oil Mixtures for Biofuels Production. *Bioresour. Technol.* **2009**, *100*, 3036–3042. [CrossRef]

8. Xu, J.; Jiang, J.; Chen, J.; Sun, Y. Biofuel Production from Catalytic Cracking of Woody Oils. *Bioresour. Technol.* **2010**, *101*, 5586–5591. [CrossRef]

9. Sriningsih, W.; Saerodji, M.G.; Trisunaryanti, W.; Triyono; Armunanto, R.; Falah, I.I. Fuel Production from LDPE Plastic Waste over Natural Zeolite Supported Ni, Ni-Mo, Co and Co-Mo Metals. *Procedia Environ. Sci.* **2014**, *20*, 215–224. [CrossRef]

10. Khowatimy, F.A.; Priastomo, Y.; Febriyanti, E.; Riyantoko, H.; Trisunaryanti, W. Study of Waste Lubricant Hydrocracking into Fuel Fraction over the Combination of Y-Zeolite and ZnO Catalyst. *Procedia Environ. Sci.* **2014**, *20*, 225–234. [CrossRef]

11. Twaiq, F.A.; Mohamed, A.R.; Bhatia, S. Liquid Hydrocarbon Fuels from Palm Oil by Catalytic Cracking over Aluminosilicate Mesoporous Catalysts with Various Si/Al Ratios. *Microporous Mesoporous Mater.* **2003**, *64*, 95–107. [CrossRef]

12. Twaiq, F.A.; Zabidi, N.A.M.; Mohamed, A.R.; Bhatia, S. Catalytic Conversion of Palm Oil over Mesoporous Aluminosilicate MCM-41 for the Production of Liquid Hydrocarbon Fuels. *Fuel Process. Technol.* **2003**, *84*, 105–120. [CrossRef]

13. Sang, O.Y. Biofuel Production from Catalytic Cracking of Palm Oil. *Energy Sources* **2003**, *25*, 859–869. [CrossRef]

14. Degnan, T.F., Jr. Applications of Zeolites in Petroleum Refining. *Top. Catal.* **2000**, *13*, 349–356. [CrossRef]

15. Nagim, I.A.; Kulkarni, K.S.; Kulkarni, A.D. Impact of Zeolites in Petroleum Industries. *J. Eng. Res. Stud.* **2011**, *2*, 272–275.

16. Kusdarto, K. Potency of Zeolite in Indonesia. *J. Zeolit Indones.* **2008**, *7*, 78–87.

17. Sihombing, J.L.; Gea, S.; Pulungan, A.N.; Agusnar, H.; Wirjosentono, B.; Hutapea, Y.A. The Characterization of Sarulla Natural Zeolite Crystal and Its Morphological Structure. *AIP Conf. Proc.* **2018**, *2049*, 020062. [CrossRef]

18. Sihombing, J.L.; Gea, S.; Kembaren, A.; Sabani; Pulungan, A.N.; Wibowo, A.A.; Wirjosentono, B. Activity Assays of Calcinated Sarulla Natural Zeolite (Snz-Cal) in Catalytic Hydrocracking Rubber Seed Oil. *J. Phys. Conf. Ser.* **2018**, *1116*, 042035. [CrossRef]

19. Parkhomchuk, E.V.; Lysikov, A.I.; Okunev, A.G.; Parunin, P.D.; Semeikina, V.S.; Ayupov, A.B.; Trunova, V.A.; Parmon, V.N. Meso/Macroporous CoMo Alumina Pellets for Hydrotreating of Heavy Oil. *Ind. Eng. Chem. Res.* **2013**, *52*, 17117–17125. [CrossRef]

20. Pashigreva, A.V.; Bukhtiyarova, G.A.; Klimov, O.V.; Chesalov, Y.A.; Litvak, G.S.; Noskov, A.S. Activity and Sulfidation Behavior of the CoMo/Al$_2$O$_3$ Hydrotreating Catalyst: The Effect of Drying Conditions. *Catal. Today* **2010**, *149*, 19–27. [CrossRef]

21. Semeykina, V.S.; Parkhomchuk, E.V.; Polukhin, A.V.; Parunin, P.D.; Lysikov, A.I.; Ayupov, A.B.; Cherepanova, S.V.; Kanazhevskiy, V.V.; Kaichev, V.V.; Glazneva, T.S.; et al. CoMoNi Catalyst Texture and Surface Properties in Heavy Oil Processing. Part I: Hierarchical Macro/Mesoporous Alumina Support. *Ind. Eng. Chem. Res.* **2016**, *55*, 3535–3545. [CrossRef]

22. Trisunaryanti, W.; Syoufian, A.; Purwono, S. Characterization and Modification of Indonesian Natural Zeolite for Hydrocracking of Waste Lubricant Oil into Liquid Fuel Fraction. *J. Chem. Chem. Eng.* **2013**, *7*, 175.

23. Gultom, F.; Wirjosentono, B.; Thamrin; Nainggolan, H.; Eddiyanto. Preparation and Characterization of North Sumatera Natural Zeolite Polyurethane Nanocomposite Foams for Light-Weight Engineering Materials. *Procedia Chem.* **2016**, *19*, 1007–1013. [CrossRef]

24. Sadek, R.; Chalupka, K.A.; Mierczynski, P.; Rynkowski, J.; Gurgul, J.; Dzwigaj, S. Cobalt Based Catalysts Supported on Two Kinds of Beta Zeolite for Application in Fischer-Tropsch Synthesis. *Catalysts* **2019**, *9*, 497. [CrossRef]

25. Shen, H.; Yao, B.; Zhang, J.; Zhu, X.; Xiang, X.; Zhou, X.; Zu, X. Effect of Thickness of Molybdenum Nano-Interlayer on Cohesion between Molybdenum/Titanium Multilayer Film and Silicon Substrate. *Nanomaterials* **2019**, *9*, 616. [CrossRef] [PubMed]

26. Pérez-Rodríguez, S.; García, G.; Calvillo, L.; Celorrio, V.; Pastor, E.; Lázaro, M.J. Carbon-Supported Fe Catalysts for CO$_2$ Electroreduction to High-Added Value Products: A DEMS Study: Effect of the Functionalization of the Support. *Int. J. Electrochem.* **2011**, *2011*. [CrossRef]

27. Kumar, K.B.; Raji, P. Synthesis and Characterization of Nano Zinc Oxide by Sol Gel Spin Coating. *Recent Res. Sci. Technol.* **2011**, *3*, 48–52.

28. Zhang, A.M.; Han, D.C.; Zhu, Z.Q.; Lee, J.W.; Rhee, H.K. Synthesis and Catalytic Application of Ni-Supported Carbon Nanotubes for n-Heptane Cracking. *Korean J. Chem. Eng.* **2003**, *20*, 649–652. [CrossRef]

29. Ding, L.; Zheng, Y.; Yang, H.; Parviz, R. LCO Hydrotreating with Mo-Ni and W-Ni Supported on Nano- and Micro-Sized Zeolite Beta. *Appl. Catal. A Gen.* **2009**, *353*, 17–23. [CrossRef]

30. Looi, P.Y.; Tye, C.T.; Mohamed, A.R. Reactions of Used Motor Oil and Residual Oil Using Mesoporous Mo/Al$_2$O$_3$ Catalyst. *J. Inst. Eng. Malays.* **2013**, *74*, 21–27.

31. Looi, P.Y.; Mohamed, A.R.; Tye, C.T. Hydrocracking of Residual Oil Using Molybdenum Supported over Mesoporous Alumina as a Catalyst. *Chem. Eng. J.* **2012**, *181–182*, 717–724. [CrossRef]
32. Ghosh, U.; Kulkarni, K.; Kulkarni, A.D.; Chaudhari, P.L. Review—Hydrocracking Using Different Catalysts. *Chem. Process Eng. Res.* **2015**, *34*, 51–55.